Image Analysis for Hen Egg Classification and Size Estimation

Supawadee Chaivivatrakul[1*] and Jednipat Moonrinta[2]
[1]Smart Engineering Agriculture Program, Faculty of Agriculture, Ubon Ratchathani University, Warin Chamrap, Ubon Ratchathani, Thailand
[2]Asian Institute of Technology, Klong Luang, Pathumthani, Thailand
E-mail: supawadee.c@ubu.ac.th*, jednipat.moonrinta@ait.asia

Received: July 11, 2025 / Revised: November 17, 2025 / Accepted: February 2, 2026

***Abstract*—Egg size and shape are critical parameters in the poultry industry's quality grading and consumer assessment. This study presents an automated image-based system to classify and estimate hen egg size, improving quality control and operational efficiency. We assembled a dataset of 150 hen eggs under Thai agricultural standards. We employed two primary image processing techniques: binary thresholding and maximum likelihood. Binary thresholding segmented egg images based on pixel intensity values, while the maximum likelihood approach—utilizing the HSV (Hue, Saturation, and Value) color space—effectively discriminated egg regions from the background. For geometric analysis, least-squares ellipse fitting and RANSAC (Random Sample Consensus) algorithms were applied to estimate egg dimensions. The classification results showed that binary thresholding achieved true positive rates of 95% and 94% on the training and test datasets, respectively, at a threshold of 0.55. The maximum likelihood method outperformed this approach, achieving classification true positive rates of 97% and 96% on the training and test datasets, respectively. Shape estimation also demonstrated high reliability, with accuracies exceeding 95% and reaching above 98%. These findings suggest that the proposed system is both accurate and practical for automated egg quality assessment in industrial settings.**

***Index Terms*—Classification, Detection, Egg Size, Segmentation, Shape**

I. Introduction

In the modern poultry industry, grading is a fundamental mechanism for improving production efficiency and ensuring product quality, making effective detection and classification systems essential to secure market value and satisfy consumers. These tasks have been performed manually, are labor-intensive and time-consuming, and are prone to subjective variability, which undermines quality control. While an alternative mechanical grading system offers a more accurate, consistent, and faster method, it increases the risk of egg damage, affecting product quality [1], [2].

The industry has sought appropriate quality-control technology, and one non-destructive approach is image processing. Researchers have applied this method effectively across various procedures and platforms [3]. One study compared a machine learning algorithm and image processing to classify white egg size. The decision tree returned the highest result on their dataset [4]. Another study proposed a method to predict egg surface area and volume. Image analysis was used to obtain egg area, and an artificial neural network and regression were used to predict the results [5]. The modern deep learning approach was adopted and applied to single-view images to analyze and return the major and minor axes of the dataset. They used a complex algorithm that required significant resources and returned highly accurate results [6]. An introduction of a non-destructive method to calculate the volume and surface area of avian eggs using two-dimensional digital imaging and image processing. They proposed a method to transform the egg's contour into standard geometric shapes (sphere, ellipsoid, or egg-shaped ovoid), then apply established geometric formulas based on image-derived measurements (egg length and projected area) [7]. Another study by this research group developed universal mathematical formulas to calculate the volume and surface area of eggs of various shapes. To the previous weakness of precise mathematical descriptions for complex shapes, especially pyriform (pear-shaped) eggs. The proposed method analyzed a progression of egg shapes from spheres to ovoid and pyriform forms, and derived equations applicable to all avian egg geometries. The outcome produced universal formulas suitable for precise, nondestructive measurement. This work is valuable for ornithology, evolutionary biology, and the poultry industry. Supports improved breeding,

incubation, and quality [8]. Previous studies showed that image processing and machine learning have high potential to predict egg size with high accuracy. This study proposes an automatic method for classifying and estimating hen egg shape to achieve high accuracy and computational efficiency. Moreover, the proposed method has less impact on the eggs. Egg size is strongly related to weight standards and can be used to cross-check quality control. An image analysis pipeline combines detection and classification using binary thresholding and maximum likelihood approaches, with accurate dimensional estimates using an elliptical fitting algorithm based on RANSAC (Random Sample Consensus).

II. Materials and Methods

This section outlines the procedures and techniques employed to develop an automated system for hen egg detection, classification, and size estimation using image processing methods. The workflow includes collecting and preparing a dataset of hen egg images, followed by two approaches—binary thresholding and the maximum likelihood method—for egg detection. Next, the system classifies eggs by pixel count and estimates their geometric dimensions using ellipse-fitting techniques. Each stage was designed to ensure computational efficiency, accuracy, and applicability to real-world conditions in poultry production environments. Fig. 1 shows the system overview.

A. Datasets

We collected a dataset of 150 hen eggs and categorized them into five standard size classes—No. 0 through No. 4—based on the Thai agricultural standard for egg grading [9]. Each class contained 30 eggs, resulting in a balanced dataset.

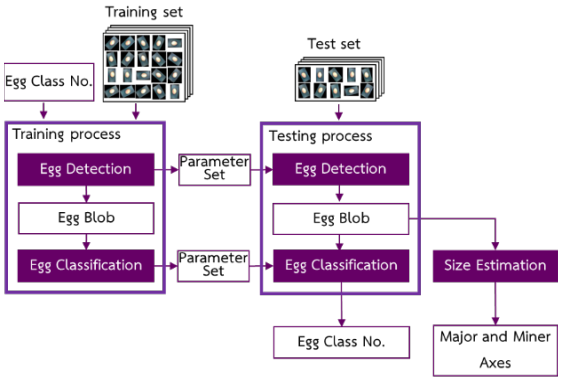


Fig. 1. System overview

For each class, 20 eggs (66.67%) were allocated to the training set and 10 eggs (33.33%) to the test set, ensuring consistent class representation across both subsets for reliable model training and evaluation (Table I). This simple proposed method requires a small dataset to demonstrate the solution, reducing computation cost and improving efficiency.

Hen egg standard in Thailand, No. 0, jumbo size, weight more than 70 g., No. 1 extra-large size, weight more than 65 g. to 70 g., No. 2 large size, weight more than 60 g. to 65 g., No. 3 medium size weight more than 55 g. to 60 g., No. 4 small size weight more than 50 g. to 55 g, and No. 5 pewee size weight more than 45 g. to 50 g. [9].

For the dataset of 150 hen egg images, each egg was taken as an image from the same angle; then the image was rotated 1- 180 degrees randomly and rescaled to get 4 datasets as 320×180 px, 160×90 px, 80×45 px, and 40×23 px, as shown in Fig. 2.

TABLE I
Dataset Proportion

Egg No.	Images in the Dataset		
	Training Set	**Test Set**	**Total**
0	20 eggs (66.67%)	10 eggs (33.33%)	30 eggs (100.00%)
1	20 eggs (66.67%)	10 eggs (33.33%)	30 eggs (100.00%)
2	20 eggs (66.67%)	10 eggs (33.33%)	30 eggs (100.00%)
3	20 eggs (66.67%)	10 eggs (33.33%)	30 eggs (100.00%)
4	20 eggs (66.67%)	10 eggs (33.33%)	30 eggs (100.00%)
Total	**100 Eggs (66.67%)**	**50 Eggs (33.33%)**	**150 Eggs (100.00%)**

B. Egg Detection

We provide 2 methods for egg detection: Binary thresholding and maximum likelihood, adopted from Chaivivatrakul [10].

1) Binary Thresholding

The binary thresholding steps include inputting an original color image, converting it to a binary image, applying a closing operation, and performing a connected-component step. Fig. 3 shows a sample output of each step.

2) Maximum Likelihood

In the maximum likelihood method, pixel values are used to calculate posterior values based on the HSV (Hue, Saturation, and Value) color model for foreground and background, as in equation (1) [11]. Fig. 4 shows a sample output of each step: Input an image, posterior calculation to return egg pixels, closing operation, and connected component.

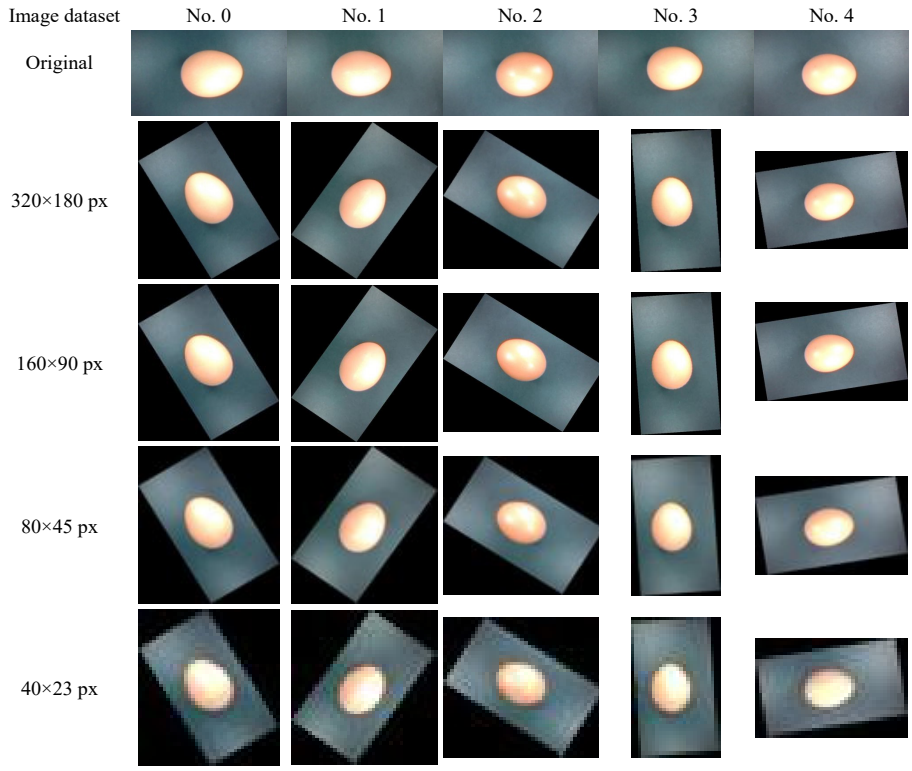


Fig. 2. Sample images of the 4 datasets

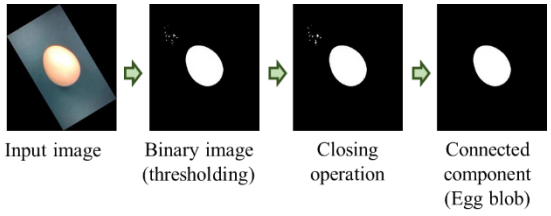


Fig. 3. Binary thresholding steps

$$P(E|x) = \frac{P(x|E)P(E)}{P(x)} \quad (1)$$

$P(E|x)$ is the probability of an egg pixel given a point x. $P(x|E)$ is the probability of a point x given an egg pixel. $P(E)$ is the probability of an egg pixel. $P(x)$ is the probability of a point x.

C. Egg Classification

Egg classes include No. 0, No. 1, No. 2, No. 3, and No. 4. The number of pixels from the detection result is used to assign egg class No. based on equations (2)-(5).

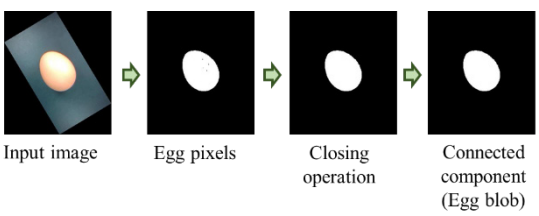


Fig. 4. Maximum likelihood steps

$$max_n = \frac{mintrain_{n+1} + maxtrain_n}{2} \quad (2)$$

$$min_n = \frac{mintrain_n + maxtrain_{n-1}}{2} \quad (3)$$

$$max_0 = maxtrain_0 \quad (4)$$

$$min_4 = mintrain_4 - 50 \quad (5)$$

n is a class No. min_n is the minimum number of pixels of class No. n in the training set. max_n is the maximum number of pixels of class No. n in the training set. $mintrain_n$ is the minimum number of pixels of class No. n in the training set. $maxtrain_{n-1}$ is the maximum number of pixels of class No. n-1 in the training set.

Formulas for classification evaluation values, the true positive rate (TP rate), the false negative rate (FN rate), the true negative rate (TN rate), the false positive rate (FP rate), Accuracy, Precision, Recall, and F-score, are provided in equations (6)-(13).

$$TP\ rate = \frac{TP}{TP+FN} \times 100 \quad (6)$$

$$FN\ rate = \frac{FN}{TP+FN} \times 100 \quad (7)$$

$$TN\ rate = \frac{TN}{TN+FP} \times 100 \quad (8)$$

$$FP\ rate = \frac{FP}{TN+FP} \times 100 \quad (9)$$

$$Accuracy = \frac{TP+TN}{TP+FN+TN+FP} \times 100 \quad (10)$$

$$Precision = \frac{TP}{TP+FP} \quad (11)$$

$$Recall = \frac{TP}{TP+FN} \quad (12)$$

$$F - score = 2 \times \frac{Precision \times Recall}{Precision + Recall} \quad (13)$$

TP is true positive, TN is true negative, FP is false positive, FN is false negative.

D. Size Estimation

We estimate the major and minor axes to estimate size. Based on the symmetrical ellipsoid assumption for egg shape, the ellipse fitting is applied to search for the major and minor axes. Algorithm 1 and Fig. 5 show the ellipse-fitting algorithm. We modified the implementation from the MATLAB File Exchange [12], [13]. Equations (14)-(17) provide the size-estimation formula.

Algorithm 1. Ransac-Ellipse-Fitting

Input: I_e: egg mask image
Output: a: major axis length
b: minor axis length
1: P_e ←SAMPLING-EGG-EDGE-POINTS(I_e,5)
2: ▶sampling 5 points on the edge of the egg mask image
3: E_j←LEAST-SQUARE-ELLIPSE-FITTING(P_e)
4: ▶j is the loop number; E_j is an ellipse for loop j
5: d_j←DISTANCE-ERROR(E_j ,P_e)
6: ▶the average perpendicular distance of all edge points P_e to the ellipse E_j
7: If d_j > 0.5 and loop j < 80
8: Go to step 1
9: If d_j <= 0.5
10: E_t←E_j
11: ▶ E_t is the taken ellipse
12: If loop j = 80
13: E_t← E_s
14: ▶E_s is the smallest average perpendicular distance ellipse
15: a, b←MAJOR-MINOR-AXIS(E_t)
16: return a,b

$$l = \frac{1}{2}\left(\frac{\sum_{e=1}^{n}\frac{h_e}{a_e}}{m} + \frac{\sum_{e=1}^{n}\frac{w_e}{b_e}}{m}\right) \quad (14)$$

$$k_e = a_e \times l \quad (15)$$

$$v_e = b_e \times l \quad (16)$$

$$r_e = \frac{k_e}{v_e} \quad (17)$$

l is the pixel size in millimeters. h_e is the height or major axis of egg e in millimeters. w_e is the width or minor axis of egg e in millimeters. a_e is the estimated ellipse major axis in pixels of egg e. b_e is the estimated ellipse minor axis in pixels of egg e. n is the number of data. k_e is the estimated egg major axis in millimeters of egg e. v_e is the estimated egg minor axis in millimeters of egg e. r_e is the estimated aspect ratio (major axis / minor axis) in millimeters of egg e.

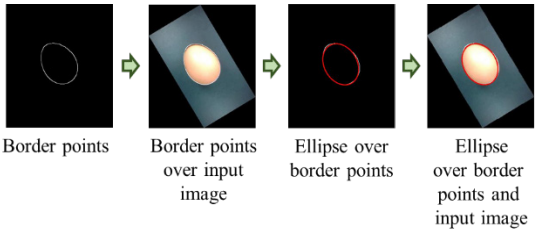


Fig. 5. RANSAC ellipse fitting steps

III. Results

The following subsections present the detection and classification results for binary thresholding and maximum likelihood, as well as the size estimation results. We chose the TP rate as the main criterion for this multi-class classification to avoid unbalanced learning effects across classes.

A. Binary Thresholding

We used the 320×180 px dataset, the highest resolution among the 4 collected datasets, and tested different threshold settings. We set the threshold to 0.50, 0.55, 0.60, 0.65, and 0.70, the disk-structure element radius to 2, and the minimum number of pixels in a connected component to 400 px.

We use image intensity to segment the background and the object. We use a grid search to find an appropriate intensity threshold, and since the 0.05 interval yields different results, we use this interval for the experiment.

Fig. 6 shows the detection sample results for binary thresholding. We evaluated the binary thresholding method at five threshold values (0.50, 0.55, 0.60, 0.65, and 0.70) using a 320×180 px dataset. Table II presents the classification results for both training and test sets, including TP rate, FN rate, TN rate, FP rate, accuracy, precision, recall, and F-score. The results show a marked improvement as the threshold increased from 0.50 to 0.55, with true positive rates rising from 27.00% to 95.00% on the training set and from 20.00% to 94.00% on the test set. A threshold of 0.55 yielded the highest overall true positive rate, making it the optimal setting for this dataset.

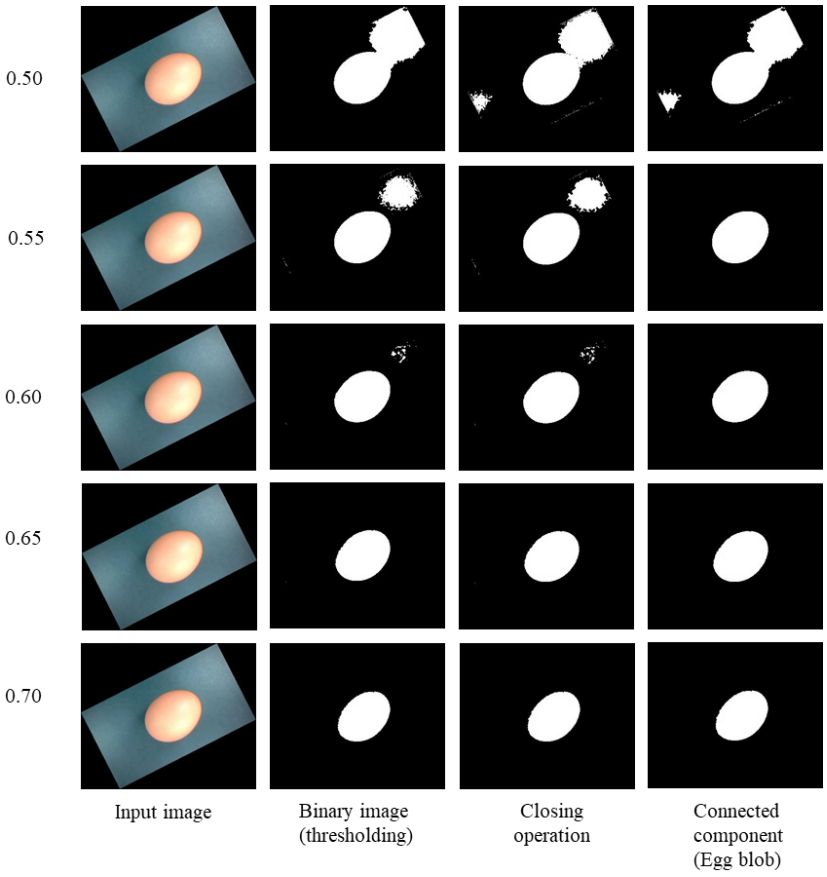


Fig. 6. Samples of the binary thresholding results with 5 threshold settings

TABLE II
CLASSIFICATION RESULTS OF BINARY THRESHOLDING ON 320×180 PX DATASET

Threshold		TP Rate (%)	FN Rate (%)	TN Rate (%)	FP Rate (%)	Accuracy	Precision	Recall	F-Score
0.50	Training Set	27.00	73.00	81.75	18.25	70.80	0.2700	0.2700	0.2700
	Test Set	20.00	80.00	80.00	20.00	68.00	0.2000	0.2000	0.2000
0.55	Training Set	95.00	5.00	98.75	1.25	98.00	0.9500	0.9500	0.9500
	Test Set	94.00	6.00	98.50	1.50	97.60	0.9400	0.9400	0.9400
0.60	Training Set	91.00	9.00	97.75	2.25	96.40	0.9100	0.9100	0.9100
	Test Set	90.00	10.00	97.50	2.50	96.00	0.9000	0.9000	0.9000
0.65	Training Set	83.00	17.00	95.75	4.25	93.20	0.8300	0.8300	0.8300
	Test Set	86.54	13.46	96.63	3.37	94.62	0.8654	0.8654	0.8654
0.70	Training Set	67.00	33.00	91.75	8.25	86.80	0.6700	0.6700	0.6700
	Test Set	74.00	26.00	93.50	6.50	89.60	0.7400	0.7400	0.7400

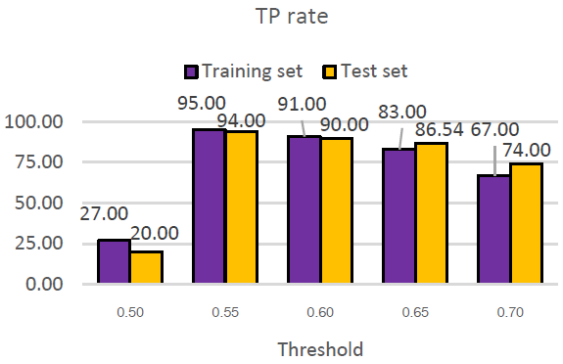


Fig. 7. TP rate of binary threshold classification results

As shown in Fig. 7, the classification TP rate began to decline beyond the 0.55 threshold. Specifically, the TP rate dropped to 91.00% at threshold 0.60, 83.00% at 0.65, and further declined to 67.00% at 0.70 for the training set. A similar pattern emerged in the test set, confirming that 0.55 represents a performance peak before over-segmentation or under-segmentation reduces the classifier's evaluation value.

Fig. 8 illustrates the confusion matrices for the binary threshold of 0.55. In both the training (Fig. 8a) and test (Fig. 8b) sets, the classifier shows strong diagonal dominance, indicating reliable class-specific predictions. Egg classes No. 0, No. 1, and No. 2 showed the highest recognition rates, while some minor confusion was observed in distinguishing class No. 3 and No. 4. Due to the number of pixels of class No.3 and No.4 being close compared to class No.1 and No.2, this confusion was observed, suggesting room for improvement through additional feature extraction or post-processing refinement.

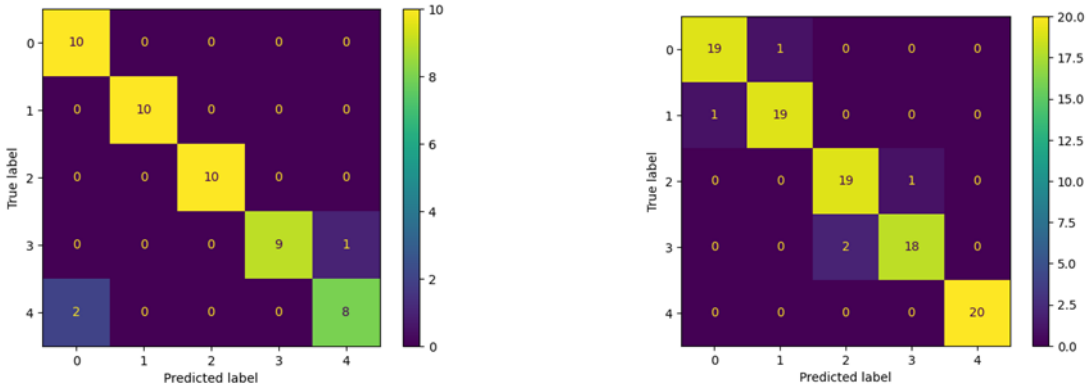


Fig. 8. Confusion matrix for the binary thresholding of 0.55 on a 320×180 px dataset (a) training set, (b) test set

B. *Maximum Likelihood*

We applied the maximum likelihood classification approach across four image resolutions: 320×180, 160×90, 80×45, and 40×23 pixels. Table III outlines the adaptive parameter sets used for each resolution, showing a decreasing disk-structure element radius and minimum pixel threshold as image resolution decreases. This scale-sensitive tuning ensured optimal region segmentation, enabling the model to balance between spatial detail and noise reduction.

TABLE III
PARAMETER SET FOR MAXIMUM LIKELIHOOD

Dataset	Radius for Disk-Structure Element	Minimum Pixel
320×180 px	4	200
160×90 px	2	100
80×45 px	1	50
40×23 px	1	25

Fig. 9 displays representative samples from the training dataset, showcasing the separability of egg and background pixels. Fig. 10 illustrates the visual results from the classification pipeline at each resolution. Table IV and Fig. 11 summarize the classification TP rate across datasets. At the highest resolution (320×180 px), the maximum likelihood method yielded an exceptional TP rate—97.00% for the training set and 96.00% for the test set. Performance declined gradually as resolution decreased, with test-set TP rates dropping to 86.00%, 78.00%, and 52.00% for 160×90, 80×45, and 40×23 px, respectively. Notably, egg Nos. 0, 1, and 4 consistently achieved high recognition rates across all resolutions, while Egg Nos. 2 and 3 performed worse, especially at lower resolutions.

Figs. 12-15 present the confusion matrices for each dataset. In the 320×180 px matrix (Fig. 12), the classification is highly accurate with minimal confusion across classes. As the resolution drops, the matrices for 160×90 px (Fig. 13), 80×45 px (Fig. 14),

and especially 40×23 px (Fig. 15), reveal increasing misclassifications, particularly between visually similar egg categories. This decline is attributed to information loss from resolution degradation, highlighting the maximum likelihood method's dependence on resolution.



(a) (b)

Fig. 9. Maximum likelihood, sample of training set for (a) egg pixels and (b) background pixels

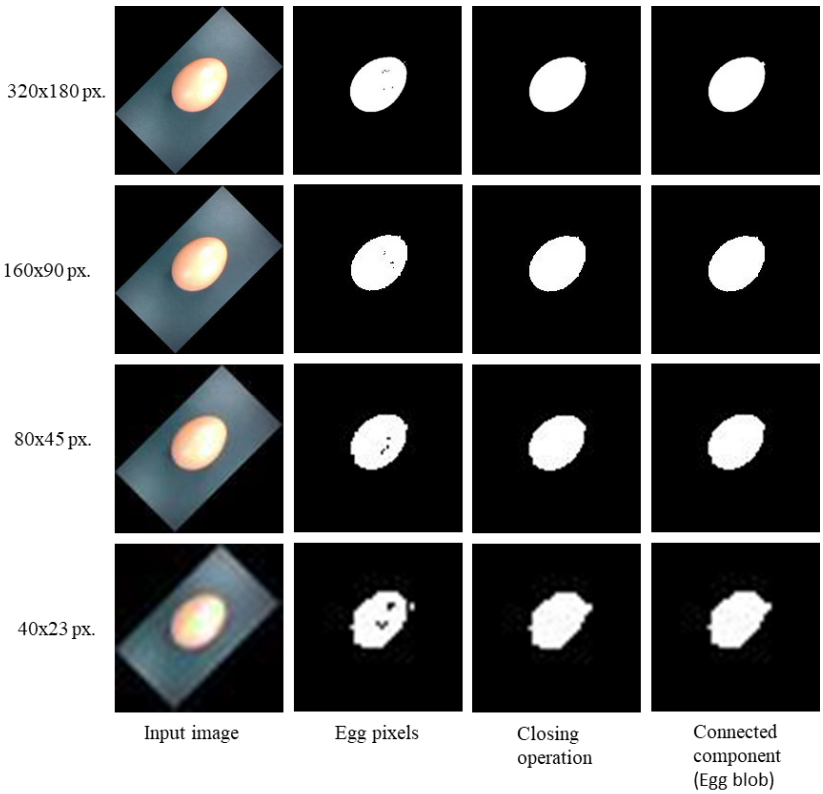


Fig. 10. Samples of the maximum likelihood results on 4 datasets

TABLE IV
CLASSIFICATION RESULTS OF MAXIMUM LIKELIHOOD ON 4 DATASETS

Dataset		TP Rate (%)	FN Rate (%)	TN Rate (%)	FP Rate (%)	Accuracy (%)	Precision	Recall	F-Score
320×180 px	Training set	97.00	3.00	99.25	0.75	98.80	0.9700	0.9700	0.9700
	Test set	96.00	4.00	99.00	1.00	98.40	0.9600	0.9600	0.9600
160×90 px	Training set	89.00	11.00	97.25	2.75	95.60	0.8900	0.8900	0.8900
	Test set	86.00	14.00	96.50	3.50	94.40	0.8600	0.8600	0.8600
80×45 px	Training set	83.00	17.00	95.75	4.25	93.20	0.8300	0.8300	0.8300
	Test set	78.00	22.00	94.50	5.50	91.20	0.7800	0.7800	0.7800
40×23 px	Training set	62.00	38.00	90.50	9.50	84.80	0.6200	0.6200	0.6200
	Test set	52.00	48.00	88.00	12.00	80.80	0.5200	0.5200	0.5200

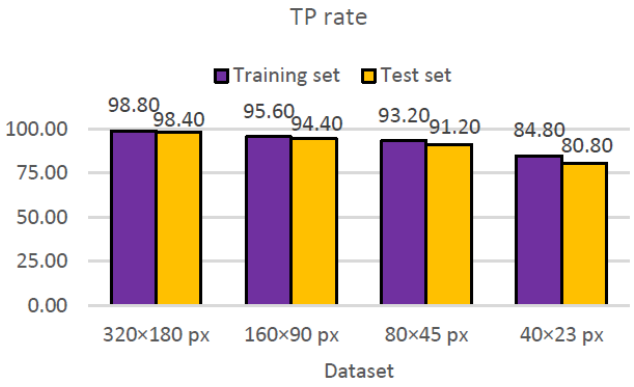


Fig. 11. Classification results of maximum likelihood

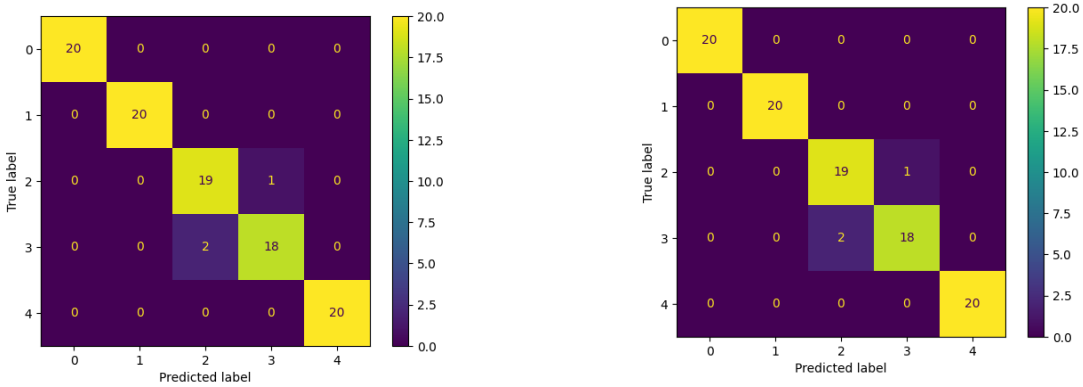


Fig. 12. Confusion matrix of 320×180 px dataset (a) training set, (b) test set

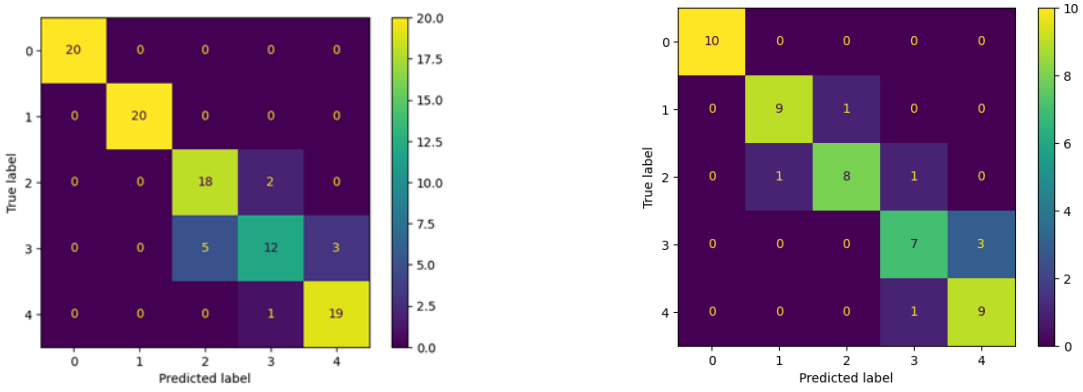
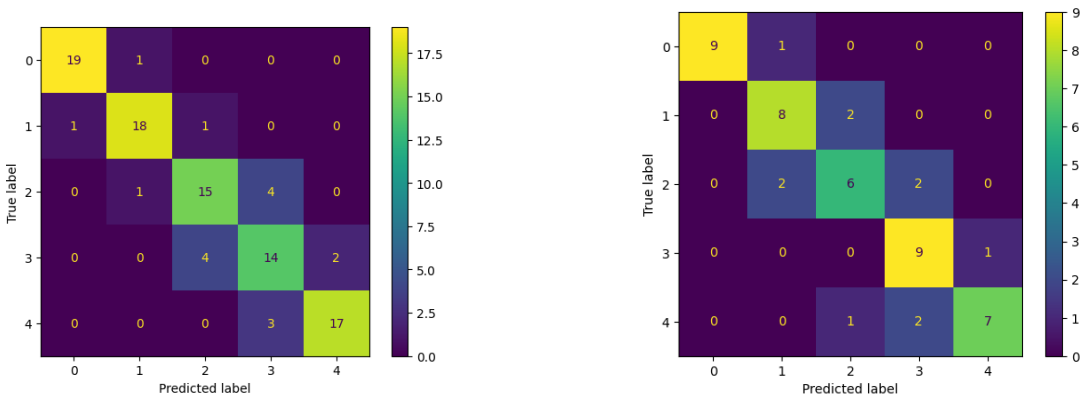
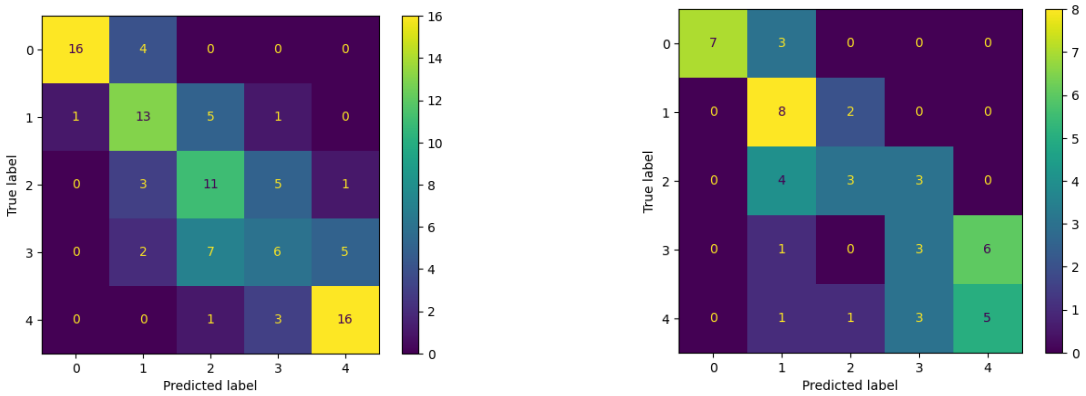


Fig. 13. Confusion matrix of 160×90 px dataset (a) training set, (b) test set



(a) (b)

Fig. 14. Confusion matrix of 80×45 px dataset: (a) training set, (b) test set



(a) (b)

Fig. 15. Confusion matrix of 40×23 px dataset: (a) training set, (b) test set

TABLE V
MAJOR AXIS AND MINOR AXIS RESULTS

Dataset	Accuracy Training Set			Accuracy Test Set		
	Major Axis	Minor Axis	Major Axis/ Minor Axis	Major Axis	Minor Axis	Major Axis/ Minor Axis
320×180 px	98.81	99.07	98.33	98.86	99.12	98.40
160×90 px	98.59	98.67	98.02	98.50	98.92	98.28
80×45 px	97.80	97.95	96.78	97.76	97.87	96.92
40×23 px	95.57	95.79	93.01	95.49	95.63	92.41

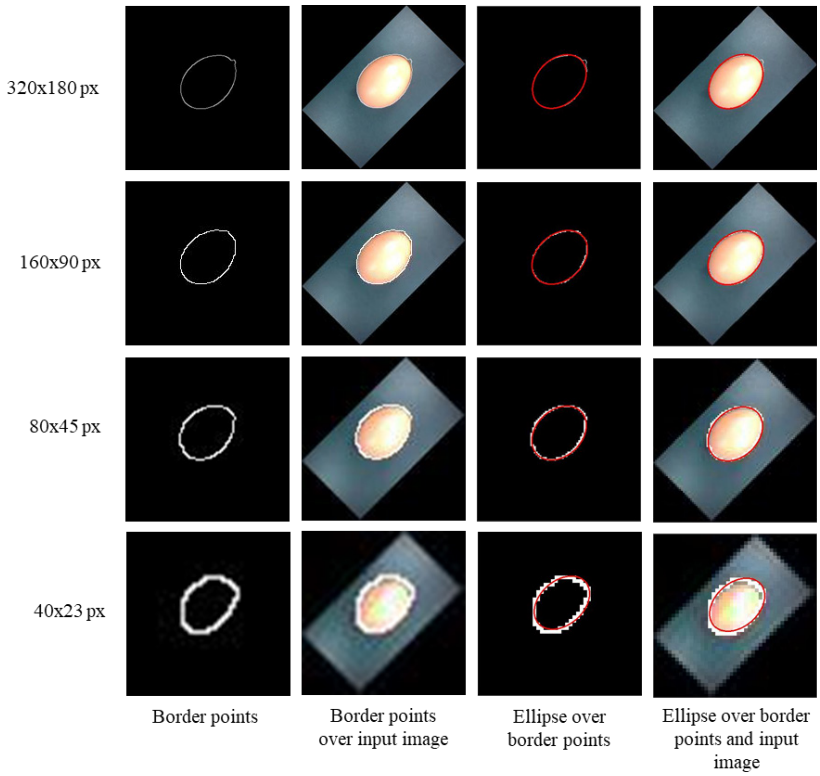


Fig. 16. Samples of the RANSAC ellipse-fitting results on 4 datasets

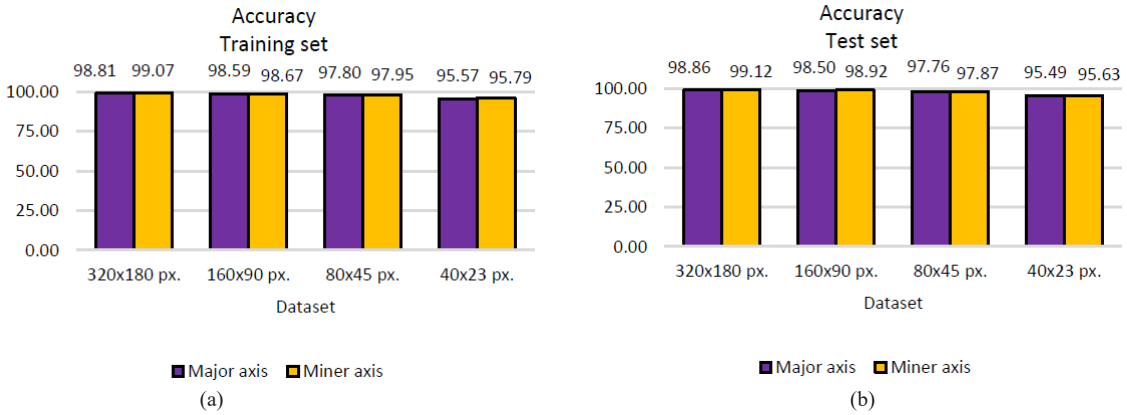


Fig. 17. Major axis and minor axis accuracy of ellipse fitting for the 320×180 px dataset (a) training set, (b) test set

IV. Conclusion and Discussion

In this paper, we looked at two main aspects of hen egg image analysis: binary thresholding and maximum likelihood estimation, which are used to detect and classify objects. We then applied RANSAC ellipse fitting to determine egg size. We assessed the accuracy, computational speed, and robustness of the methods by testing them on images at different resolutions.

Binary thresholding is a simple detection method with low processing overhead. The ideal threshold value of 0.55 yielded the most accurate results, with a TP rate of 95% for the training set and 94% for the test set. This shows that the background and foreground can be identified under the right conditions. Nevertheless, excessive or inadequate segmentation caused performance to deteriorate rapidly at suboptimal threshold levels, and the process relied heavily on the selected threshold. Because binary thresholding performs poorly when either the background or the lighting changes frequently, it should be used only where these factors are constant.

Maximum likelihood classification, on the other hand, worked better and could handle a wider range of shapes and lighting conditions. It performed better with a resolution of 320×180 px. The test set's TP rate was 96%, and the training set's was 97%. This dataset resolution also produced the best results across the other evaluation metrics: the highest TN

rate, accuracy, precision, recall, and F-score, and the lowest FP and FN rates. As resolution decreased, the TP rate dropped, although it stayed at 62% and 52% at 40×23 pixels, and the other evaluation values decreased similarly. Eggs were more likely to be assigned to the appropriate class for eggs No. 0, No. 1, and No. 4. Grouping classes with similar traits or slight differences, such as Nos. 2 and 3, was more challenging.

In applications requiring size estimation, the RANSAC ellipse-fitting method worked effectively. The accuracy of measurements on the major and minor axes was more than 98% at 320×180 px resolution. Even at the lowest resolution, accuracy remained above 95%. This illustrates that RANSAC can be used for real-time size estimation in embedded vision systems with constrained processing power and performs well with low resolution.

Overall, the results show that a key design challenge is balancing categorization strength with computational efficiency. Binary thresholding works well but is sensitive to parameter settings and cannot adjust automatically. Maximum probability approaches generalize more but require slightly more processing power. In contrast, shape estimates from RANSAC-based elliptical fitting are reliably precise and consistent. For this reason, it is useful for tasks like grading, sorting, and spotting errors.

Industries today need to balance usability, scalability, and performance in their image analysis systems. Because of their ease of use and low resource requirements, traditional computer vision techniques such as SIFT, SURF, template matching, and decision trees remain useful. As a result, they work well on the edge and in static environments [4]-[8], [14]. These typically cannot handle very complex problems.

However, deep learning methods such as Convolutional Neural Networks (CNNs), Vision Transformers (ViTs), and high-performance object detectors like YOLOv9 are the most accurate and versatile. On key benchmarks such as Cityscapes, COCO, and ImageNet, they perform well [15], [19]. They also reported strong results on an in-house collected agricultural dataset [20]. In real-time or embedded systems, they are rarely used because they require large amounts of memory, computational power, and labeled data [15], [16], [21], [22].

Hybrid approaches combine lightweight neural inference with classical preprocessing, such as quantized models or edge-optimized architectures, to address these limitations. These solutions are ideal because they enable real-time, scalable, and accurate visual inspection systems. When choosing a method, we need to consider latency, hardware limitations, data availability, and industry standards, especially in sectors like manufacturing and autonomous robots. This improves quality control and builds customer confidence.

Future studies will test the effectiveness of these strategies in a conveyor-based egg grading system to determine how well they perform in real factories. Adding additional egg types, sizes, and lighting conditions to the dataset will greatly improve the model's performance. Additionally, hybrid solutions that combine traditional image processing with novel deep learning architectures can enhance system accuracy and adaptability when resources are limited.

Acknowledgment

We thank the Faculty of Agriculture, Ubon Ratchathani University, and agricultural communities for supporting this research by providing facilities and resources.

References

[1] J. Alikhanov, Z. Shynybay, A. Moldazhanov, A. Kulmak-Hambetova, and P. Daskalov, "Machine control system operation for automatic sorting of eggs into categories," in *Proc. 5th Int. Sci. Congr. Agricultural Machinery*, 2017, pp. 222-226.

[2] I. Bagus, K. Dzinavatongaet, E. Chimana, and C. Mabuyaye, "Design and development of an IoT-based chicken egg sorting prototype based on egg weight," in *Proc. 3rd Conf. IDB Bali*, 2024, pp. 356-362.

[3] K. Limpadapun and T. Borirak, "Advancing industrial inspection through image processing techniques with OpenCV," *EAU Heritage Journal Science and Technology*, vol. 19, no. 1, pp. 63-76, Apr. 2025, https://he01.tci-thaijo.org/index.php/EAUHJSci/article/view/275593/186733

[4] D. M. Mendoza, R. G. De Luna, C. F. C. Navarro, M. R. Isada, L. Tuason, and J. M. P. Macadag-Um, "Standardized Sizing through Machine Learning (SML): Utilizing decision tree algorithm to classify white chicken egg sizes," in *Proc. IEEE Region 10 Humanitarian Technology Conf. (R10-HTC)*, 2024. pp. 66-71, https://doi.org/10.1109/R10-HTC59322.2024.10778850

[5] M. Sedghi and M. Ghaderi, "Digital analysis of egg surface area and volume: Effects of longitudinal axis, maximum breadth and weight," *Inf. Process. Agric.*, vol. 10, no. 2, pp. 229-239, Jun. 2023, https://doi.org/10.1016/j.inpa.2022.01.003

[6] C. Liu et al., "Single-view measurement method for egg size based on small-batch images," *Foods*, vol. 12, no. 5, Mar. 2023, https://doi.org/10.3390/foods12050936

[7] V. G. Narushin, G. Lu, J. Cugley, M. N. Romanov, and D. K. Griffin, "A 2-D imaging-assisted geometrical transformation method for non-destructive evaluation of the volume and surface area of avian eggs," *Food Control*, vol. 112, Jun. 2020, https://doi.org/10.1016/j.foodcont.2020.107112

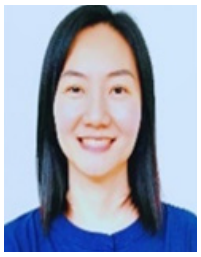
[8] V. G. Narushin, J. P. Kent, A. Salamon, M. N. Romanov, and D. K. Griffin, "Density of egg interior: Looking inside an egg while keeping it intact," *Innov. Food Sci. Emerg. Technol.*, vol. 87, Jul. 2023, https://doi.org/10.1016/j.ifset.2023.103387

[9] National Bureau of Agricultural Commodity and Food Standards, *Thai Agricultural Standard (TAS 6702-2005): Hen egg*. Bangkok, Thailand: ACFS, 2005. [Online]. Available:https://faolex.fao.org/docs/pdf/tha166331.pdf

[10] S. Chaivivatrakul, "Automatic assessment of seed germination percentage," *Eng. J.*, vol. 24, no. 4, pp. 85-96, Jul. 2020, https://doi.org/10.4186/ej.2020.24.4.85

[11] K. P. Murphy, *Machine Learning: A Probabilistic Perspective*. Cambridge, MA, USA: MIT Press, 2012, pp. 1-1104.

[12] R. Brown, "fitellipse.m," *MATLAB Central File Exchange*, 2025. [Online]. Available: https://www.mathworks.com/matlabcentral/fileexchange/15125-fitellipse-m [Accessed Jun. 10, 2025].
[13] M. Arthington, "Distance from points to an ellipse," *MATLAB Central File Exchange*, 2025. [Online]. Available: https://www.mathworks.com/matlabcentral/fileexchange/26261-distance-from-points-to-an-ellipse [Accessed: Jun. 10, 2025].
[14] M. Isik, "Comprehensive empirical evaluation of feature extractors in computer vision," *Peer J Comput. Sci.*, vol. 10, p. e2415, Nov. 2024, https://doi.org/10.7717/peerj-cs.2415
[15] Y. Liu et al., "A survey of visual transformers," *IEEE Trans. Neural Netw. Learn. Syst.*, vol. 35, no. 6, 2024, https://doi.org/10.1109/TNNLS.2022.3227717
[16] R. Azad et al., "Advances in medical image analysis with vision transformers: A comprehensive review," *Med. Image Anal.*, vol. 91, Art. no. 103000, Jan. 2024, https://www.sciencedirect.com/science/article/pii/S1361841523002608
[17] C. -Y. Wang, I.-H. Yeh, and H. -Y. M. Liao, "YOLOv9: Learning what you want to learn using programmable gradient information," in *Proc. Eur. Conf. Comput. Vis. (ECCV)*, 2024, pp. 1-21.
[18] Z. Zong, G. Song, and Y. Liu, "DETRs with collaborative hybrid assignments training," in *Proc. IEEE Int. Conf. Comput. Vis. (ICCV)*, 2023, pp. 6748-6758.
[19] E. Xie, W. Wang, Z. Yu, A. Anandkumar, J. M. Alvarez, and P. Luo, "SegFormer: Simple and efficient design for semantic segmentation with transformers," in *Adv. Neural Inf. Process. Syst*., 2021, pp. 12077-12090.
[20] K. Orkphol, K. Satianpakiranakorn, J. Chaihuadjaroen, and T. Valeeprakhon, "A transfer learning-based deep convolutional neural network approach for white shrimp abnormality classification," *Int. Sci. J. Eng. Technol. (ISJET)*, vol. 8, no. 2, Dec. 2024.
[21] M. Tan and Q. V. Le, "EfficientNetV2: Smaller models and faster training," in *Proc. 38th Int. Conf. Mach. Learn. (ICML)*, 2021, pp. 10096-10106.
[22] Z. Luo, W. Yang, Y. Yuan, R. Gou, and X. Li, "Semantic segmentation of agricultural images: A survey," *Inf. Process. Agric.,* vol. 11, no. 2, pp. 172-186, Jun. 2024, https://www.sciencedirect.com/science/article/pii/S2214317323000112



Supawadee Chaivivatrakul received the B.S. and M. S. degrees in computer science from Chiang Mai University, Chiang Mai, Thailand, in 1999 and 2003, respectively, and the Ph.D. in computer science from Asian Institute of Technology, Bangkok, Thailand, in 2014. She was a visiting scholar in Agriculture and Biosystems Engineering, Iowa State University, IA, USA, in 2010. She received a full scholarship from NSTDA for her Ph.D. Since 2005, she has been a lecturer in Information Technology for Agriculture and Rural Development and Smart Engineering Agriculture at the Faculty of Agriculture, Ubon Ratchathani University.



Jednipat Moonrinta received the B.Eng. degree in computer engineering from Chiang Mai University, Chiang Mai, Thailand, in 2008, and an M. Eng. Degree in computer science from Asian Institute of Technology (AIT), Pathumthani, Thailand, in 2010.

He worked as a research associate at the AIT Vision Lab from 2010 to 2015 before starting his doctoral studies. He is currently pursuing a Ph.D. degree in computer science at AIT and working at the AI Center. His research interests include computer vision, deep learning, and intelligent systems.